ORIGINAL RESEARCH

Neonatal Pulmonary Macrophage Depletion Coupled to Defective Mucus Clearance Increases Susceptibility to Pneumonia and Alters Pulmonary Immune Responses

Yogesh Saini[1,2], Kristen J. Wilkinson[1], Kristy A. Terrell[1], Kimberlie A. Burns[1], Alessandra Livraghi-Butrico[1], Claire M. Doerschuk[1], Wanda K. O'Neal[1], and Richard C. Boucher[1]

[1]Marsico Lung Institute/University of North Carolina Cystic Fibrosis Center, School of Medicine, University of North Carolina at Chapel Hill, Chapel Hill, North Carolina; and [2]Department of Comparative Biomedical Sciences, School of Veterinary Medicine, Louisiana State University, Baton Rouge, Louisiana

Abstract

Resident immune cells (e.g., macrophages [MΦs]) and airway mucus clearance both contribute to a healthy lung environment. To investigate interactions between pulmonary MΦ function and defective mucus clearance, a genetic model of lysozyme M (LysM) promoter–mediated MΦ depletion was generated, characterized, and crossed with the sodium channel β subunit transgenic (Scnn1b-Tg) mouse model of defective mucus clearance. Diphtheria toxin A–mediated depletion of LysM[+] pulmonary MΦs in wild-type mice with normal mucus clearance resulted in lethal pneumonia in 24% of neonates. The pneumonias were dominated by Pasteurella pneumotropica and accompanied by emaciation, neutrophilic inflammation, and elevated Th1 cytokines. The incidence of emaciation and pneumonia reached 51% when LysM[+] MΦ depletion was superimposed on the airway mucus clearance defect of Scnn1b-Tg mice. In LysM[+] MΦ-depleted Scnn1b-Tg mice, pneumonias were associated with a broader spectrum of bacterial species and a significant reduction in airway mucus plugging. Bacterial burden (CFUs) was comparable between Scnn1b-Tg and nonpneumonic LysM[+] MΦ-depleted Scnn1b-Tg mice. However, the nonpneumonic LysM[+] MΦ-depleted Scnn1b-Tg mice exhibited increased airway inflammation, the presence of neutrophilic infiltration, and increased levels of inflammatory cytokines in bronchoalveolar lavage fluid compared with Scnn1b-Tg mice. Collectively, these data identify key MΦ–mucus clearance interactions with respect to both infectious and inflammatory components of muco-obstructive lung disease.

Keywords: alveolar macrophages; macrophage depletion; sodium channel β subunit transgenic mice; airway mucus obstruction; airway inflammation

Airway and alveolar host defense is mediated by multiple interconnected mechanisms, including airway mucociliary clearance and innate immune responses. Innate immune responses are performed by multiple cell populations (e.g., resident pulmonary macrophages [MΦs]) and secretion of soluble antimicrobial factors in both airway and alveolar regions. Primary defects in each of these layers of defense can produce disease and/or compensatory responses in other defenses, which may be beneficial to the host, or harmful, if they persist for protracted intervals. Elucidation of the interactions between defense mechanisms that maintain lung health is complex and requires direct experimental testing.

Mucus hyperconcentration, mucostasis, and mucus plugging are key pathophysiologic events in many airway diseases, including chronic obstructive pulmonary disease and cystic fibrosis. Although persistent microbial infection in static mucus can produce chronic inflammation, the potential proinflammatory effects of static, but sterile, mucus are poorly

understood. Resident MΦs are key sentinel cells for both airway and alveolar surfaces, and their responses to failed mucus clearance are likely to contribute to disease pathogenesis. Upon an encounter with inhaled particles or organisms, pulmonary MΦs assist in clearance and dampen or promote local inflammatory responses, depending upon their activation status and the nature of the stimulus. Like failed mucus clearance, loss of normal MΦ function has been reported to produce important pulmonary consequences, including pneumonia (1–3). We hypothesize that pulmonary MΦs are key pulmonary defense cells that respond to mucus obstruction, becoming activated in response to failed clearance by sensing and responding to hyperconcentrated mucus itself, and/or exogenous and endogenous inflammatory stimuli trapped and concentrated within adherent mucus.

To investigate the interplay between reduced mucociliary clearance and the MΦ components of host defense, we used the well characterized, epithelial sodium channel β subunit (*Scnn1b*) transgenic mouse (*Scnn1b*-Tg). In this model, the overexpression of *Scnn1b* transgene is controlled by the rat club cell secretory protein (CCSP) promoter (2.25-Kb 5′ flanking region of CCSP gene, also known as *Scgb1a1*), which targets expression to airway club cells (previously referred to as Clara cells) with sporadic expression in alveolar type II cells (4, 5). Previously published studies have characterized the cell-specific expression of *Scnn1b* transgene and the resulting airway surface liquid dehydration (5, 6). The neonatal and adult muco-obstructive airways disease (5, 6) produced by airway surface liquid dehydration is characterized by inflammation that includes increased MΦ size, persistent airway neutrophilia, and bronchial-associated lymphoid tissues (5–7). Morphologic (6, 7), functional (8), and recent gene array (9) studies indicate that pulmonary MΦs are robustly activated soon after birth in *Scnn1b*-Tg mice, suggesting that they contribute significantly to the development of lung inflammation.

To characterize the contribution of MΦs to neonatal *Scnn1b*-Tg mouse lung disease, mice with MΦ depletion were generated using lysozyme M (LysM) cyclization recombinase (Cre)–mediated expression of gene encoding diphtheria toxin A (DTA) subunit. The LysM promoter was selected for these studies because of its high level of expression in pulmonary MΦs (10). The functional consequences of DTA expression on pulmonary MΦ populations were evaluated during the neonatal period in wild-type (WT) mice and with *Scnn1b*-Tg expression. Putative "positive" compensatory consequences of MΦ depletion on the neonatal *Scnn1b*-Tg lung phenotype (e.g., reduced inflammation) were sought in parallel with potential "negative" effects of compromising these key protective cells (e.g., increased on bacterial infection).

Materials and Methods

Transgenic Mice and Animal Husbandry

All animal protocols were approved by the Institutional Animal Care and Use Committee at the University of North Carolina (Chapel Hill, NC). The four distinct transgenic lines used are detailed subsequently here, and include: (*1*) LysM-Cre mice expressing Cre from the myeloid-specific LysM promoter; (*2*) membrane-targeted Tomato (mTOM)/ membrane-targeted enhanced green fluorescent protein (mEGFP)-floxed reporter mice where the Gt(ROSA)26Sor (a gene locus controlling constitutive expression of transgenes/constructs, abbreviated ROSA promoter for this article) locus expresses reporter gene mTOM (red) in the absence of Cre and mEGFP (green) upon Cre activation; (*3*) DTA-floxed mice with DTA expression induced by Cre activation; and (*4*) *Scnn1b*-Tg mice, which develop mucus obstruction. Studies were performed on neonates (5–7 days old), as indicated in figures and text.

Generation of Transgenic Mice

All mice used in the study were maintained in hot-washed, individually ventilated micro-isolator cages on a 12-hour dark/ light cycle, and were fed a regular diet and water *ad libitum*. LysM-Cre mice (B6.129P2-*Lyz2*$^{tm1(cre)Ifo}$/J), mTOM/ mEGFP reporter mice (B6.129(Cg)Gt (ROSA) 26Sortm4(ACTB-tdTomato,- EGFP)Luo/J) and DTA-floxed (B6.129P2*Gt(ROSA) 26Sor*$^{tm1(DTA)Lky}$/J) were procured from Jackson Laboratory (Bar Harbor, ME). At the time of procurement, LysM-Cre mice were on mixed C57Bl/6N and C57Bl/6J background, whereas mTOM/mEGFP

reporter mice and DTA-floxed mice were on C57Bl/6J background. *Scnn1b*-Tg mice used in the study were C57Bl/6N congenic.

Generation of mouse models of fluorescent marker-labeled macrophages, macrophage depletion and crosses with Scnn1b-Tg mice. The myeloid cell–specific LysM promoter was used to drive expression of Cre in the myeloid lineage. The LysM-Cre mice used in this work have a targeted insertion of the Cre transgene in the exon 1 region of the LysM locus (11). To minimize the negative effect of Cre toxicity, we only generated and analyzed animals with a single copy of the Cre transgene, a strategy that also assured functionality of at least one allele of the LysM gene.

Generation and use of macrophage-reporter mice. LysM-Cre mice were crossed with the Gt(ROSA)26Sor-mTOM/mEGFP dual-reporter mouse strain. This strain contains an engineered transgene that is controlled by the ROSA promoter. In mice without Cre, the locus of crossover in phage 1 (LoxP)-flanked mTOM transgene/polyA stop cassette (red fluorescence at the membrane) is expressed from the ROSA promoter, and the mEGFP transgene (green fluorescence at the membrane) is silent due to the presence of LoxP-flanked poly(A) stop cassette (12). The presence of Cre results in recombination-mediated removal of flanked mTOM transgene/polyA stop cassette and induction of mEGFP transgene expression. Using this dual reporter transgene crossed to LysM-Cre mice, a mouse model was generated where LysM-Cre–positive cells would express the mEGFP.

Generation and use of LysM$^+$ MΦ-depleted mice. Similar to the Gt(ROSA) 26Sor–mTOM/mEGFP dual-reporter strain, the Gt(ROSA)26Sor-DTA mouse strain contains an engineered transgene (i.e., a loxP-flanked neomycin/PolyA stop cassette) proximal to the DTA transgene that is controlled by the ROSA promoter (13). To achieve depletion of MΦs, LysM-Cre mice were mated with the Gt(ROSA)26Sor-DTA mice. The presence of Cre in the Gt(ROSA) 26Sor-DTA mouse cells results in recombination-mediated removal of the neomycin/polyA stop cassette and, thus, induction of DTA transgene expression (13). LysM$^+$ MΦ-depleted mice were generated by mating LysM-Cre$^{+/+}$ mTOM/mEGFP$^{+/+}$ mice with DTA$^{+/-}$ mice, producing triple transgenic mice with a reporter transgene in which Cre expressing cells expressed mEGFP and DTA, simultaneously.

LysM⁺ MΦ-depleted Scnn1b-Tg mice.
LysM-Cre$^{+/+}$ Scnn1b-Tg$^{+/-}$ mice were generated and mated with DTA$^{+/-}$ mice to generate LysM$^+$ MΦ-depleted Scnn1b-Tg animals. LysM$^+$ MΦ-depleted Scnn1b-Tg mice with a MΦ-specific reporter transgene were generated by mating LysM-Cre$^{+/+}$ mTOM/mEGFP$^{+/+}$ mice with DTA$^{+/-}$ Scnn1b-Tg$^{+/-}$ mice.

PCR Genotyping
Genomic DNA extraction from tail tissue was performed using the Direct-PCR extraction reagent (Viagen Biotech, Los Angeles, CA), according to the manufacturer's instructions. Genotyping was performed by PCR for all the loci as previously published (5, 11–13). PCR conditions for all the alleles were: denaturation at 94°C for 5 minutes, 38 cycles of amplification (94°C for 45 seconds, 60°C for 45 seconds, and 72°C for 1 minute and 10 seconds, followed by a 7-minute extension at 72°C). The amplified products were electrophoresed in 2% agarose in Tris borate EDTA for 30 minutes at 200 V. The ethidium bromide–stained gels were imaged in FluorChemQ imaging system (Alpha Innotech, San Jose, CA).

Bronchoalveolar Lavage Collection and Lung Tissue Processing
Bronchoalveolar lavage fluid (BALF) was harvested for differential cell counts and microbiological analyses as previously described (14).

Fluorescence Microscopy
To harvest lung tissues for fluorescent imaging, mice were anesthetized with Avertin (2,2,2-tribromoethanol), and, after exsanguination, lungs and tracheas were exposed through a midline thoracotomy. Lungs were inflated *in situ* with 50% OCT in PBS. Whole lungs were embedded in OCT in tissue molds and frozen on dry ice. The lungs in the OCT frozen blocks were positioned to optimize longitudinal sectioning of primary bronchi. OCT-embedded frozen lung tissues were sectioned to a thickness of 5 μm on a cryostat. For fluorescent imaging, frozen sections were fixed in ice-cold acetone for 10 minutes. Fixed sections were washed twice in PBS and mounted with VECTASHIELD HardSet mounting medium with 4′,6-diamidino-2-phenylindole (Vector Labs, Burlingame, CA). Sections were observed under Olympus FV1000 MPE SIM laser scanning confocal microscope (Olympus, Pittsburgh, PA) at the University of North Carolina Michael Hooker Microscopy Facility. For the determination of mTOM$^+$ and mEGFP$^+$ cells, cytospin preparations were prepared and fixed in 10% neutral buffered formalin for 15 minutes. The fixed Cytospin slides were washed with PBS and mounted with VECTASHIELD HardSet mounting medium with 4′,6-diamidino-2-phenylindole (Vector Labs). Cytospin slides were observed under Olympus FV1000 MPE SIM laser scanning confocal microscope. mTOM$^+$

(no mEGFP label) and mEGFP$^+$ (with or without mTOM label) MΦs were counted based on morphology, as determined by differential interference contrast microscopy. A total of approximately 200 cells were counted to estimate the percentage of mTOM$^+$ and mEGFP$^+$ MΦs.

Flow Cytometry
BAL cells were collected as described previously here. Cells were fixed in a one-step fix/lyse solution (eBiosciences, San Diego, CA), washed twice in PBS, and the pellets were suspended in staining buffer. BAL cells were analyzed for the mEGFP and mTOM fluorescence with Dako CyAn (Beckman Coulter, Inc., Pasadena, CA). Flow cytometric data were analyzed using Summit software Version 4.3 (Dako, Carpinteria, CA).

Cytokine Assay on BAL
Mouse TNF-α, keratinocyte chemoattractant (KC), macrophage inflammatory protein 2 (MIP-2), MIP-1α, MIP-1β, macrophage colony–stimulating factor (M-CSF), IL-10, IL-12, IL1α, IL-17, IL-4, IL-5, IL-6, IP-10, monocyte chemotactic protein-1 (MCP-1) and LPS-induced CXC chemokine (LIX) levels were measured in cell-free BAL using a Luminex-based assay (MCYTOMAG-70K; EMD Millipore Corp., Billerica, MA), according to the manufacturer instructions.

Histopathological Slide Preparation
The 10% neutral buffered formalin–fixed lungs were paraffin embedded, and 4- to
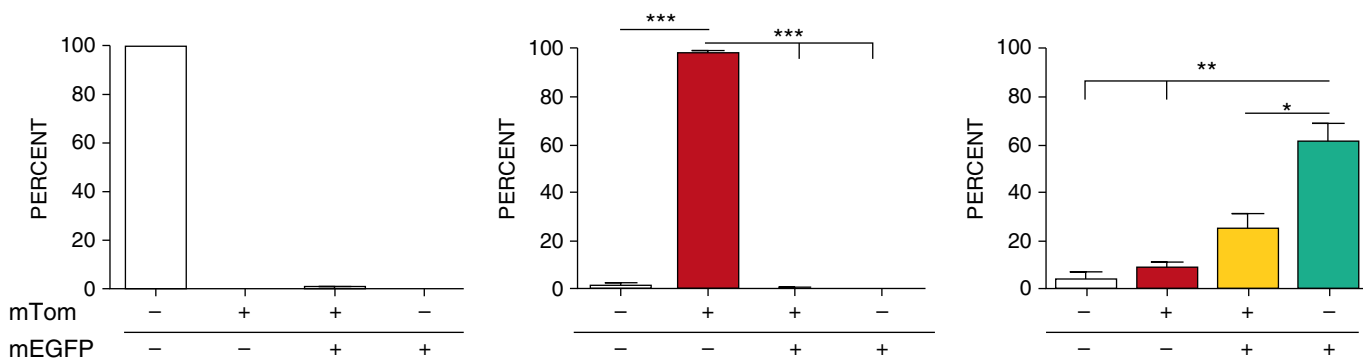

Figure 1. Lysozyme M (LysM) promoter expression activity in neonates. Flow cytometry analysis of neonatal bronchoalveolar lavage (BAL) cells harvested from LysM-cyclization recombinase (Cre)$^+$ single-transgenic mice (*left panel*), membrane-targeted Tomato (mTOM)/membrane-targeted enhanced green fluorescent protein (mEGFP)$^+$ single-transgenic mice (*middle panel*), and LysM-Cre$^+$\mTOM/mEGFP$^+$ mice (*right panel*). The results reflect the distribution of BAL cells in the four quadrants from the flow analyses (Figure E2). Gt(ROSA)26Sor (a gene locus controlling constitutive expression of transgenes/constructs, abbreviated ROSA promoter for this article) locus drives mTOM (*red*) or mEGFP (*green*) expression in the absence or presence of Cre activity, respectively. *White bars* represent percentage of cells negative for mTOM and mEGFP signal; *red bars* represent percentage of cells positive for mTOM, but negative for mEGFP signal; *yellow bars* represents percentage of cells positive for mTOM and mEGFP signal; *green bars* represents percentage of cells negative for mTOM, but positive for mEGFP signal. Data are expressed as means (±SEM). *n* = 3/group. ANOVA: *$P < 0.05$, **$P < 0.01$, ***$P < 0.001$.

6-μm-thick sections were cut. The lung tissues from 5- to 7-day-old mice were oriented to obtain longitudinal sections of primary bronchi. Sections were mounted on glass slides and stained with hematoxylin and eosin for lung morphological assessments and Alcian blue/periodic acid–Schiff for mucopolysaccharide assessment of intracellular and extracellular mucus.

Lung Histopathology

A previously reported semiquantitative grading system was used to score airway obstruction, mucus secretory cell abundance, airspace enlargement, and airway inflammation phenotypes (graded on a 0–3 scale) (14). The alveolar space consolidation phenotype was scored on the scale of 0–3: 0, no evidence of alveolar space consolidation; 1, less than 25% of left lung lobe with alveolar space consolidation; 2, ≥25–50% of the lobe with alveolar space consolidation; and 3, ≥50% of the lobe with alveolar space consolidation.

Statistical Analyses

Statistical analyses were performed using GraphPad Prism 5.0 (GraphPad Software, Inc., La Jolla, CA). One-way ANOVA followed by Tukey's *post hoc* test for multiple comparisons was used to determine significant differences among groups. *P* less than 0.05 was considered statistically significant. All data are expressed as means (±SEM).

Results

Characterization of LysM Promoter Activity in Pulmonary MΦs

Before evaluating LysM-mediated DTA depletion of pulmonary MΦs, a dual reporter LysM- Cre$^+$\mTOM/mEGFP$^+$ bitransgenic line was generated to characterize the cell specificity of LysM-Cre in our mice. Flow cytometric evaluations of mTOM- and mEGFP-expressing cells were conducted on BAL cells collected from neonatal (5–7 days old) mice expressing LysM-Cre (to target Cre expression to myeloid cells under the LysM promoter) (11), ROSA-mTOM/mEGFP (reporter construct ROSA-mTOM/mEGFP containing floxed mTOM) (12), or both transgenes (*see* Figure E1 in the online supplement). In the absence of Cre activity, owing to the polyadenylation sequence

downstream of the loxP-flanked mTOM transgene, mEGFP expression did not occur in ROSA-mTOM/mEGFP mice. However, in the presence of Cre activity, recombination-mediated excision of the mTOM region within the floxed ROSA-reporter construct simultaneously eliminated mTOM expression and thus induced mEGFP expression (Figure E1).

In the absence of LysM-Cre, ROSA-mTOM/mEGFP reporter mice exhibited robust ROSA locus expression activity in BAL cells (96% of which were MΦs [data not shown]), as indicated by mTOM$^+$ expression in approximately 98% of harvested cells (Figure 1, middle panel, and Figure E2). In contrast, robust LysM promoter–driven Cre activity in MΦs was evident by the presence of mEGFP$^+$ MΦs

in bitransgenic, Cre-expressing reporter mice (Figure 1, *right panel*). In our mice, LysM-Cre activity–induced mEGFP expression was detected in approximately 87% of neonatal pulmonary MΦs harvested by BAL.

LysM-Cre–Driven DTA Expression Alters Pulmonary MΦ Populations

The above studies indicated that approximately 87% of BAL MΦ populations could be targeted for depletion using LysM-Cre–induced recombination in a floxed ROSA-DTA allele. Therefore, a bitransgenic (LysM-Cre$^{+/+}$ ROSA-mTOM/mEGFP$^{+/+}$) line was bred to an available transgenic line with a DTA-floxed allele targeted to the ROSA locus (13) to produce triple-transgenic mice (Figure E1).
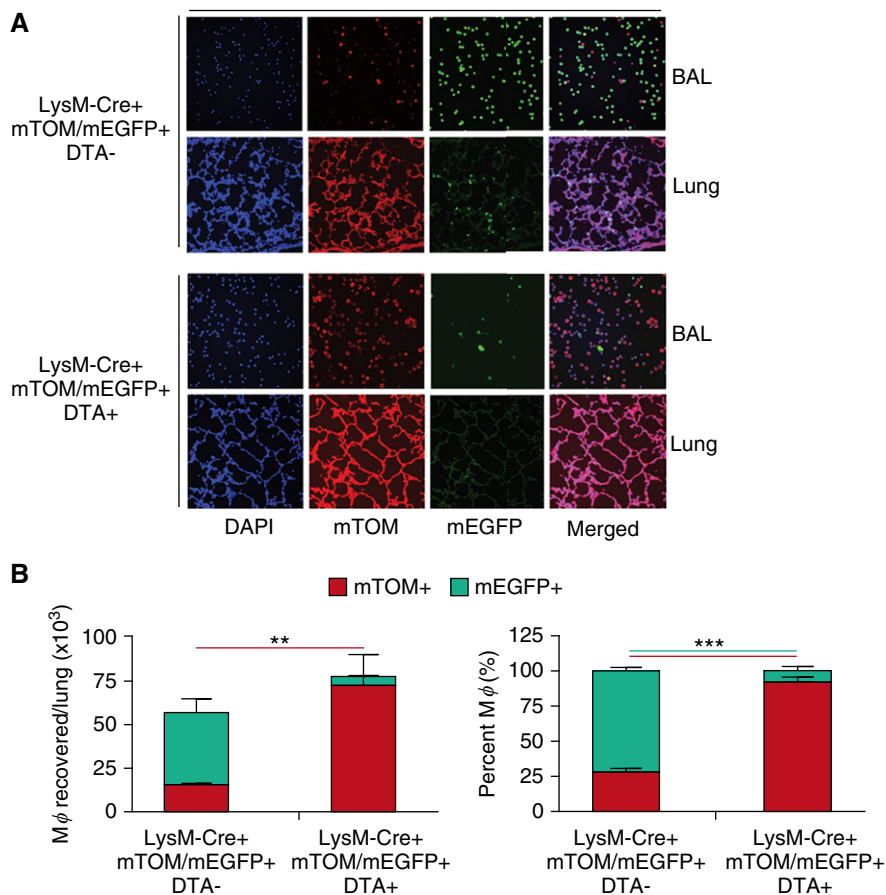

Figure 2. Diphtheria toxin A (DTA) expression targeted to pulmonary macrophages (MΦs) alters the pulmonary MΦ phenotype. BAL cytospins and histological lung sections (*A*) were evaluated for mTOM (*red*; LysM-Cre negative) or mEGFP (*green*; LysM-Cre positive) expression via fluorescence microscopy in neonates. Presence (+) or absence (−) of the transgenes is indicated to the *left* of each *panel*. Quantitative assessment (*B*) of total and percentage of MΦs expressing either mTOM or mEGFP, as determined by counting cells showing fluorescent signal on cytospins (*n* = 3–4). Data are expressed as means (±SEM). ANOVA: **P < 0.01, ***P < 0.001. DAPI, 4′,6-diamidino-2-phenylindole.

Selective breeding (*see* Supplemental Materials and Methods) generated LysM-Cre–positive, ROSA-mTOM/mEGFP–positive, ROSA-floxed DTA–positive mice, in which both mTOM/mEGFP and DTA transcription were under the control of LysM promoter–driven Cre recombination. This feature facilitated tracking of DTA-expressing cells via the simultaneous expression of mEGFP$^+$, providing the ability to monitor DTA-induced cell death using, as a readout, the proportion of mEGFP$^+$ cells in DTA$^+$ compared with DTA$^-$ lines. Triple-transgenic mice were obtained in the expected Mendelian ratios (data not shown).

Expression of the DTA transgene had clear effects on pulmonary MΦ populations. As predicted, DTA$^+$ mice exhibited a significant depletion of BAL mEGFP$^+$ MΦs compared with their DTA$^-$ counterparts (Figure 2A). However, we observed an unexpected shift in BAL cell populations with DTA expression. Compared with DTA$^-$ mice (Figure 2B), the absolute numbers and the percentage of mTOM$^+$ MΦs (defined as MΦs based on their morphology) from the DTA$^+$ mice were increased (Figure 2B). Because of the increased numbers of mTOM$^+$, the absolute MΦ numbers were not reduced in DTA$^+$ neonates (Figure 2B). Of note, BAL neutrophils were consistently raised in neonatal DTA$^+$ mice (Figure E3).

Phenotype of WT and *Scnn1b*-Tg Neonates in Presence or Absence of DTA Transgene Expression

Additional breeding was conducted to introduce the *Scnn1b*-Tg into the LysM$^+$ MΦ-depleted (DTA$^+$) line. The mice obtained from these crosses were phenotyped in the neonatal period.

Altered MΦ phenotypes in* Scnn1b-Tg *neonates with and without MΦ depletion. We first noted that the total MΦ number was increased in *Scnn1b*-Tg compared with WT mice (Figure 3A). Interestingly, the increase in MΦ numbers in *Scnn1b*-Tg mice reflected an increase in mTOM$^+$ MΦs. The total numbers of MΦs collected from LysM-Cre$^+$/mTOM/mEGFP$^+$/*Scnn1b*-Tg neonates with and without DTA expression were comparable (Figure 3). However, there were major differences in the distribution of MΦ phenotypes. DTA expression reduced the absolute number and percentage of MΦs with an active LysM promoter, as indicated by the
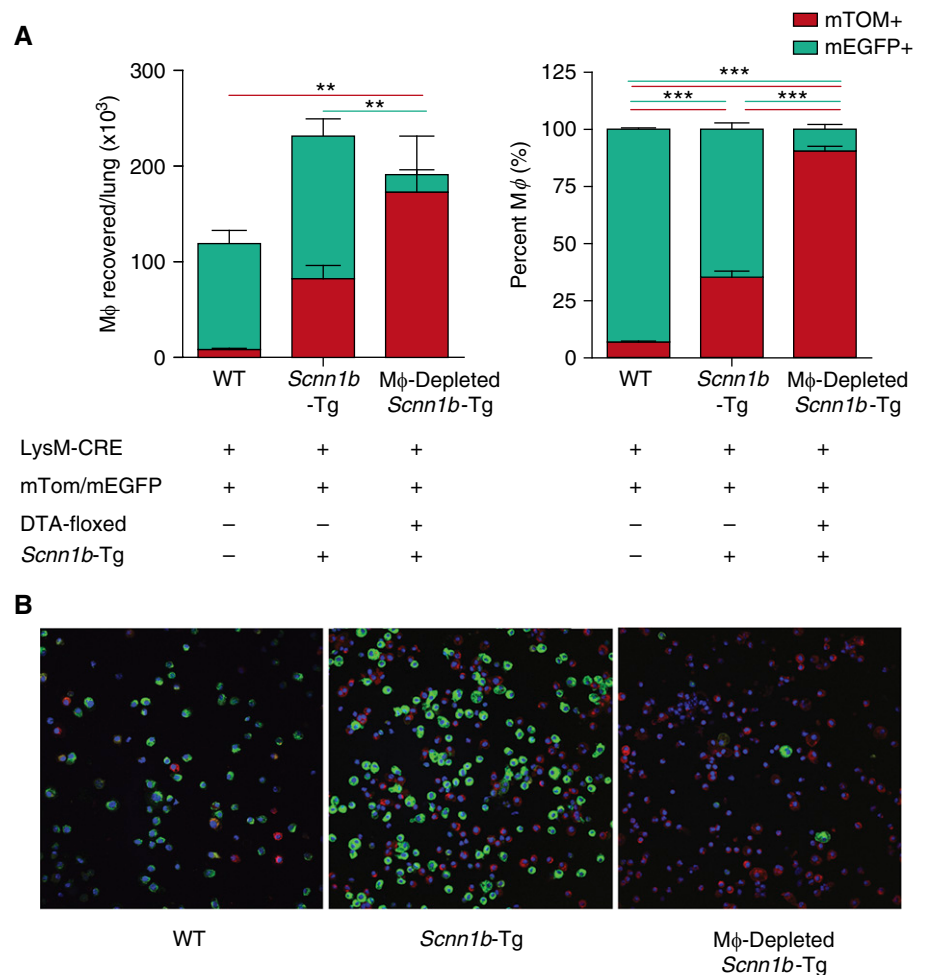
reduction in BAL mEGFP$^+$ MΦs, and an increase mTOM$^+$ BAL MΦs in DTA$^+$/*Scnn1b*-Tg neonates. Thus, in agreement with our data in DTA$^+$ WT mice (Figure 2B), DTA expression led to an absolute increase in LysM-inactive MΦs (Figure 3).

DTA$^+$ neonates were susceptible to emaciation, lung inflammation, bacterial pneumonia, and death. There were no visible phenotypic abnormalities at birth in any line. However, by 2–3 days after birth, 24% of DTA$^+$/WT neonates exhibited an emaciation phenotype defined by reduced weight gain, flaky discoloration of skin, lethargy, and eventual death (Figure 4A). No DTA$^-$/*Scnn1b*-Tg neonates exhibited emaciation, but

the prevalence of emaciation increased to 51% in DTA$^+$/*Scnn1b*-Tg neonates (Figure 4B). The severity of weight loss due to emaciation was similar between DTA$^+$/*Scnn1b*-Tg and DTA$^+$/WT neonates (Figure 4C).

DTA$^+$ neonates exhibited histologic evidence of pulmonary pathology. Histologically, there was no evidence of pathology in major nonrespiratory organs (liver, heart, intestine, spleen, and pancreas) in neonates (data not shown). In contrast, the lungs exhibited significant pathology.

Alveolar space consolidation was the key histologic finding associated with LysM$^+$ MΦ depletion in neonates (Figures 5A and 5B). Nonemaciated DTA$^+$/WT

Figure 3. Characteristics of LysM and ROSA promoter activity in sodium channel β subunit transgenic (*Scnn1b*-Tg) mouse BAL cells. (*A*) Histogram indicating the total cells (*left panel*) and percentage (*right panel*) of mTOM (*red*) or mEGFP (*green*) expressing MΦs collected from neonates in the presence (+) or absence (−) of the transgenes as indicated. DTA expression leads to increased prevalence of mTOM-positive cells in *Scnn1b*-Tg mice. Data are expressed as means (±SEM). ANOVA: **$P < 0.01$, ***$P < 0.001$. (*B*) Representative fluorescent images of BAL cells in LysM-Cre reporter neonatal mice that are wild-type (WT), DTA$^-$/*Scnn1b*-Tg, or DTA$^+$/*Scnn1b*-Tg.
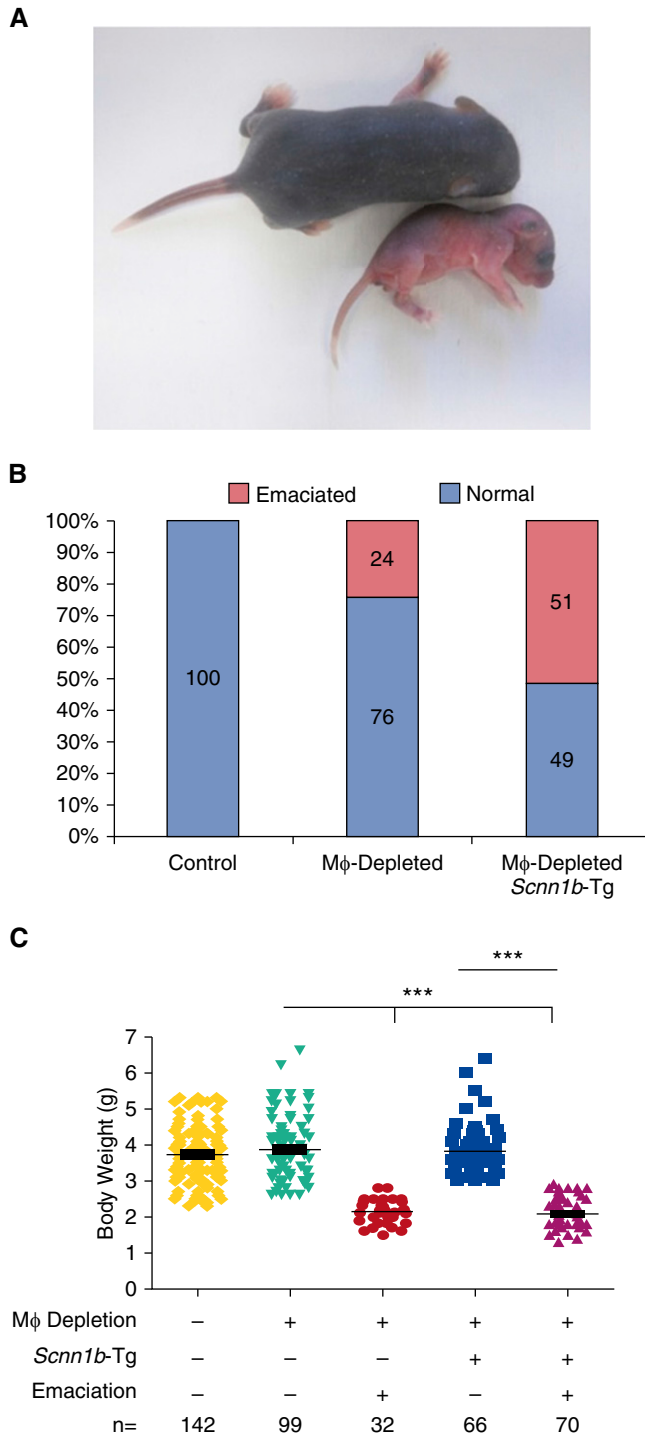
A

B

C

Figure 4. A percentage of MΦ-depleted mice become severely emaciated in the neonatal period associated with inflammatory cell influx. (*A*) The emaciation phenotype observed in the neonatal period. Both littermates are MΦ depleted, but the larger pup is not emaciated. (*B*) Percentage of mice showing the emaciation phenotype in the various transgenic mouse lines, as indicated. (*C*) Body weight in emaciated and nonemaciated mice in the transgenic mouse lines, as indicated. ANOVA: ***$P < 0.001$.

neonates exhibited mild, heterogeneous alveolar space consolidation, whereas emaciated DTA$^+$/WT neonates exhibited severe and more uniform alveolar

consolidation (Figures 5A and 5B). Consolidated alveoli were characterized by infiltrating neutrophils and enlarged, primarily apoptotic, MΦs (as determined

by *in situ* terminal deoxynucleotidyl transferase dUTP nick end labeling assay; Figure E4) that were more prominent in emaciated than in nonemaciated DTA$^+$/WT neonates. No differences in the degree of alveolar space consolidation were noted in DTA$^+$/*Scnn1b*-Tg compared with DTA$^+$/WT neonates (Figures 5A and 5B).

Airway inflammation, as assessed histologically, was significant in all neonatal DTA$^+$/WT mice compared with DTA$^-$/WT (Figure 5B). The defective mucus clearance that is a feature of *Scnn1b*-Tg mice was associated with more pronounced airway inflammation in nonemaciated and emaciated DTA$^+$/*Scnn1b*-Tg neonates compared with nonemaciated DTA$^+$/WT littermates (Figures 5A and 5B). The emaciation phenotype was strikingly associated with increased alveolar and airway inflammation in both WT and *Scnn1b*-Tg mice (Figures 5A and 5B).

Mucus obstructive phenotypes were not prominent in the airways of DTA$^+$/WT neonatal mice. Mucus plugs and increased bronchial mucus cell numbers were observed in *Scnn1b*-Tg neonates, consistent with the reported pathophysiology (5, 6). However, the extent of the mucus phenotype produced in *Scnn1b*-Tg mice was dependent upon emaciation and MΦ depletion status. Interestingly, although the degree of mucus plugging was comparable in nonemaciated DTA$^+$/*Scnn1b*-Tg and DTA$^-$/*Scnn1b*-Tg neonates, the mucus retention phenotype was markedly reduced in emaciated DTA$^+$/*Scnn1b*-Tg mice (Figures 5A and 5B).

An increase in the size of alveolar units was evident in all *Scnn1b*-Tg lines, as previously described (Figures 5A and 5B). Previous studies have demonstrated that this histological feature reflects the failed development of alveolar septa and/or the loss of alveolar walls per acinar unit (i.e., an emphysema-like phenotype) (6, 15). Visually similar alveolar space enlargement was a consistent feature in the nonconsolidated regions of emaciated DTA$^+$/WT. In DTA$^+$/*Scnn1b*-Tg mice, these lesions were observed irrespective of emaciation status (Figure 5B).

Total and differential BAL cell counts and BAL cytokine levels reflected differential responses among the experimental groups to LysM$^+$ MΦ depletion, emaciation status, and the presence or absence of *Scnn1b*-Tg expression (Figure 5; Table 1). In DTA$^+$/WT
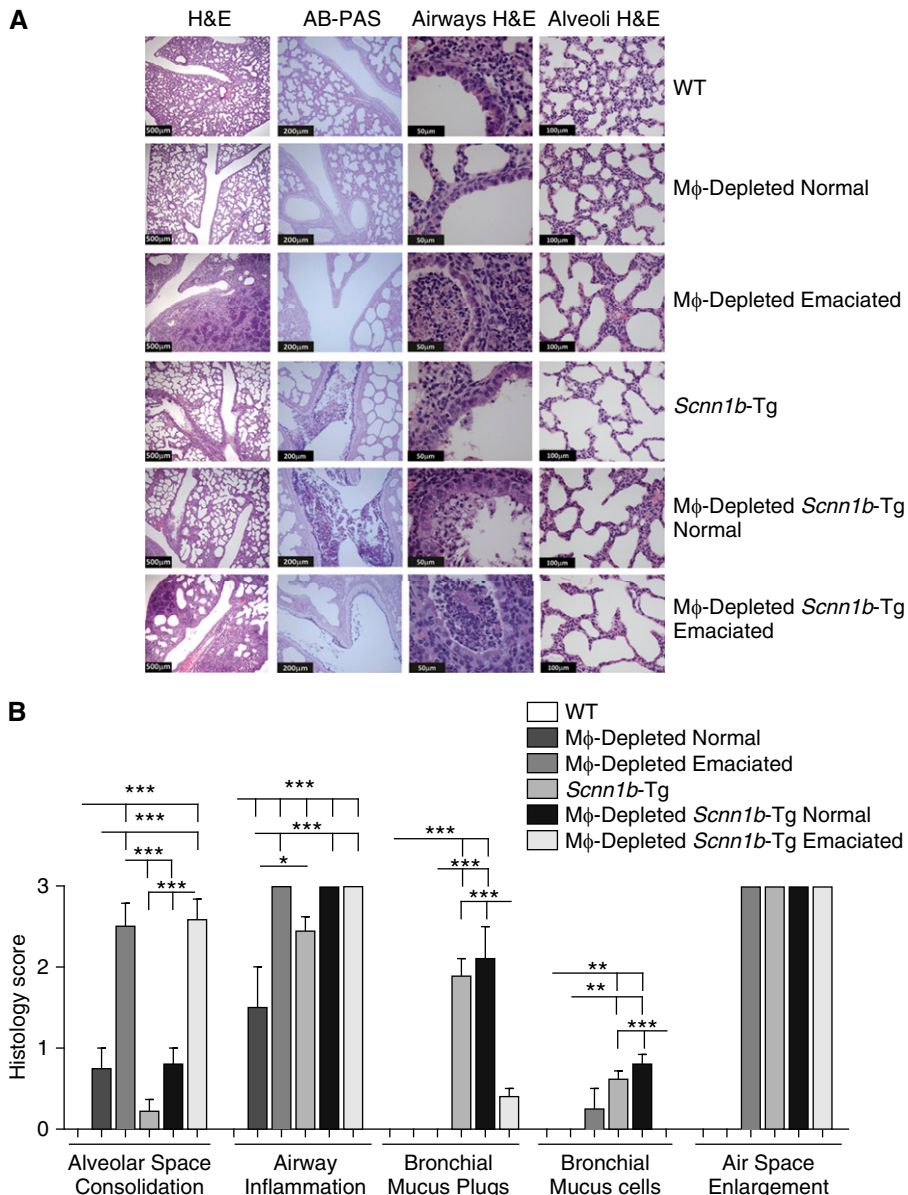
A

B

Figure 5. MΦ-depleted neonates exhibit significant pulmonary pathology. (*A*) Representative micrographs for the genotypes, as indicated. Both emaciated and nonemaciated phenotypes are shown. Hematoxylin and eosin (H&E) stain was used to highlight morphological features, whereas Alcian blue/periodic acid–Schiff (AB-PAS) stain highlights mucus substances (*dark purple*). The *scale bars* in H&E (lungs), H&E (airways), H&E stained (alveoli), and AB-PAS stained (lungs) are 500 μm, 50 μm, 100 μm, and 200 μm, respectively. (*B*) Semiquantitative histological scores for relevant clinical features of neonatal mice. Data are expressed as means (±SEM). ANOVA: *$P < 0.05$, **$P < 0.01$, ***$P < 0.001$.

were not affected by DTA expression or as a function of emaciation status compared with their WT counterparts (Figures 6A–6C). Similar to nonemaciated DTA[+]/WT or DTA[+]/*Scnn1b*-Tg neonates, BAL MΦs recovered from the emaciated counterparts were predominantly mTOM[+] (data not shown).

The BAL inflammatory mediators tested were either below the detection limit or were present at minimal concentrations in DTA[−]/WT neonates (Table 1). LysM[+] MΦ depletion in WT neonates without emaciation resulted in a significant increase in the level of the neutrophil chemokine, KC (Table 1), consistent with the BAL neutrophilia (Figures 2B and 4C, Figure E3). Consistent with our previous reports (7, 14), BAL levels of KC, MIP2, MIP1α, MIP1β, and TNF-α were elevated in DTA[−]/*Scnn1b*-Tg neonates compared with DTA[−]/WT mice. Nonemaciated DTA[+]/*Scnn1b*-Tg neonates exhibited a further elevation in the levels of these cytokines. Strikingly, the emaciation phenotype in DTA[+]/WT as well as DTA[+]/*Scnn1b*-Tg neonates was associated with a "cytokine storm," as indicated by dramatic increases in 13 of 16 measured inflammatory mediators. Interestingly, only IL-5 was significantly reduced in emaciated compared with "normal" counterparts (Table 1).

MΦ depletion leads to neonatal bacterial pneumonia. The histological, cytokine, and BAL findings in emaciated neonates suggested bacterial infection, and studies were performed to test this hypothesis. Spleen cultures were negative for all genotypes, and no culturable bacteria were isolated from BAL of DTA[−]/WT neonates. However, a sporadic (3/16), small bacterial burden was observed in the BAL from nonemaciated DTA[+]/WT neonates (Figure 7A). In striking contrast, CFU counts were consistently approximately 5 logs higher (mean CFU = 2.3×10^7) in BAL harvested from emaciated DTA[+]/WT neonates. Sequence analyses revealed that *Pasturella pneumotropica,* a common inhabitant of the mouse oropharynx (7), was the sole bacterial species culturable in emaciated DTA[+]/WT BAL (Figure 7B).

Total bacterial burden in *Scnn1b*-Tg and nonemaciated DTA[+]/*Scnn1b*-Tg neonates were comparable and represented an admixture of bacterial pathogens previously reported in *Scnn1b*-Tg mice (7). *Streptococcus* spp., *Actinobacillus* spp., and

neonates, DTA expression produced no change in total macrophage numbers compared with DTA[−]/WT neonates (Figure 6, in agreement with Figure 2B). However, total BAL cells were significantly increased in DTA[+]/WT neonates compared with DTA[−]/WT neonates due to increased neutrophil recruitment (Figures 6A–6C), consistent with cytological observations (Figure 2B and Figure E3).

Emaciated DTA[+]/WT neonates exhibited three to six times higher total cell numbers as compared with genotype-matched nonemaciated littermates, attributable not only to a large increase in neutrophil counts, but also to a small, but significant, increase in lymphocytes (Figures 6A–6C). Total BAL cells and macrophage numbers were increased in neonatal *Scnn1b*-Tg mice compared with WT mice, but total counts

Table 1. Cytokine Responses in Neonatal Mice across Designated Groups

Cytokine	WT	MΦ-Depleted WT "Normal"	MΦ-Depleted WT "Emaciated"	Scnn1b-Tg	MΦ-Depleted Scnn1b-Tg "Normal"	MΦ-Depleted Scnn1b-Tg "Emaciated"	Lower Limits of Detection
KC	2.3 ± 0.9*†	45.8 ± 28.5†‡	**1,204.0 ± 303.5**	85.4 ± 21.9*	154.8 ± 38.1‡	**1,522.0 ± 269.4**	3.0
MIP2	14.7 ± 1.4*	19.9 ± 3.6‡	**7,463.0 ± 1,365.0**	273.5 ± 64.8*	540.1 ± 137.8‡	**5,898.0 ± 1,436.0**	16.0
Mip1α	1.4 ± 0.0	1.4 ± 0.0	**9,180.0 ± 272.5***	32.4 ± 8.8	123.5 ± 56.4	**4,768.0 ± 1,576.0***	18.0
LIX	18.7 ± 0.0	18.7 ± 0.0	**799.0 ± 238.8**	20.6 ± 1.9*	200.5 ± 55.8*	**1,236.0 ± 254.2**	18.7
TNFα	0.6 ± 0.0	1.7 ± 1.1*	**355.9 ± 68.3**	11.1 ± 4.2	21.2 ± 8.4*	**502.4 ± 138.3**	3.1
IL-5	12.3 ± 5.9	26.7 ± 9.5	0.1 ± 0.0	6.7 ± 2.9	5.8 ± 3.0	0.12 ± 0.0	2.9
IL10	1.7 ± 0.2	1.1 ± 0.2	**466.9 ± 243.4**	1.5 ± 0.3	1.6 ± 0.3	**388.8 ± 168.2**	3.1
M-CSF	0.0 ± 0.0*	2.2 ± 1.3	11.8 ± 3.3	13.9 ± 1.9	15.3 ± 2.8	15.6 ± 4.5*	2.8
IL-17	0.0 ± 0.0	0.0 ± 0.0	**933.0 ± 31.4***	0.0 ± 0.0	8.8 ± 4.7	13.5 ± 4.3*	3.1
IL-6	1.4 ± 0.3*	13.9 ± 7.2	**1,620.0 ± 324.3**	10.2 ± 2.4*	17.4 ± 5.4	**1,355.0 ± 412.6**	3.2
IP10	14.2 ± 1.8	18.5 ± 7.4	**362.0 ± 37.0***	15.1 ± 2.0	34.4 ± 14.6	**189.5 ± 49.6***	3.1
MCP1	5.9 ± 0.0	5.9 ± 0.0	**426.2 ± 64.6**	5.9 ± 0.0	29.4 ± 14.5	**296.1 ± 68.9**	17.0
IL-4	1.2 ± 0.2	3.8 ± 1.2	**18.8 ± 6.1***	1.6 ± 0.3	3.43 ± 0.8	**6.7 ± 1.8***	3.2
MIP1β	15.4 ± 0.0	18.8 ± 3.3	**9,189.0 ± 925.8**	32.0 ± 9.7	204.9 ± 108.3	**6,195.0 ± 1,507.0**	18.9
IL-1α	24.9 ± 9.0	118.9 ± 78.5	**1,810.0 ± 881.3**	32.9 ± 9.6	135.9 ± 42.6	677.7 ± 354.0	18.8
IL-12	0.0 ± 0.0	0.5 ± 0.3	1.3 ± 0.9	1.8 ± 1.2	0.7 ± 0.4	0.4 ± 0.1	3.1

Definition of abbreviations: IP-10, interferon-γ-inducible protein 10; KC, keratinocyte chemoattractant; LIX, LPS-induced CXC chemokine; MΦ, macrophage; MCP, monocyte chemotactic protein; M-CSF, macrophage colony–stimulating factor; MIP, macrophage inflammatory protein; *Scnn1b*-Tg, sodium channel β subunit transgenic; WT, wild-type.
Cytokine levels (pg/ml) in bronchoalveolar lavage. *Bold text* indicates significantly higher values comparing "Normal" with "Emaciated" within the "MΦ-Depleted WT" and "MΦ-Depleted *Scnn1b*-Tg" groups. The SEM values for some cytokines were 0.0 because these cytokine levels were below detection limits and were assigned the values equal to the lowest assay detection limit. Values less than the lower limit of detections were obtained by extrapolation. $n = 5$–6, $P < 0.05$.
,†,‡Two values carrying identical designations (for example, "" or "†" or "‡") in same row represent significant difference.

P. pneumotropica, routine colonizers in *Scnn1b*-Tg neonates, were the predominant organisms in nonemaciated DTA⁺/*Scnn1b*-Tg mice. *P. pneumotropica* predominated, but was not the sole bacterial species in the emaciated DTA⁺/*Scnn1b*-Tg mice (Figure 7B). The CFU counts in emaciated DTA⁺/WT and DTA⁺/*Scnn1b*-Tg neonates were similar.

Discussion

Mucus stasis has been associated with robust MΦ activation in *Scnn1b*-Tg mice (7–9) and human lung disease (16). MΦ activation is likely critical for both the protection of the lung as a compensatory mechanism and as a significant contributor to the development of the chronic inflammatory pathology in this model. Evaluation of muco-obstructive disease development in the presence and absence of MΦs is one way to investigate the complex interrelationships between mucus stasis and MΦ function. This approach is challenging, however, as the pathophysiology associated with both MΦ depletion and mucostasis are superimposed on normal lung developmental processes in both of our

models (9). Furthermore, MΦ activation is known to be highly pleiotropic and sensitive to local environmental stimuli (17). The interpretation of *in vivo* findings to address these interrelationships is critically dependent upon the specific features of the model.

For this study, due to the early onset of lung disease in *Scnn1b*-Tg mice (5), it was necessary to develop a model that would exhibit chronic MΦ depletion starting at birth. This requirement ruled out the use of chemical-/drug-induced approaches of MΦ depletion (18–20) and necessitated genetically induced depletion of MΦs. One of the most widely used myeloid cell–restricted promoters, LysM, was selected to drive cell type–specific expression of Cre (11). The LysM promoter has been reported to be active in all myeloid cells (21), with one report indicating LysM promoter activity also in occasional alveolar epithelial type II cells (22).

In our study, LysM promoter activity in cells harvested by BAL, as indexed by Cre-mediated expression of mEGFP was age and disease dependent. Importantly, our studies identified a previously unappreciated age dependency in LysM promoter activity in BAL MΦs. Whereas a vast majority of alveolar MΦs harvested from normal adult

mice was positive for LysM promoter activity (data not shown), a significant percentage of MΦs harvested from neonatal lavages exhibited a delay in the LysM-Cre–mediated recombination in the reporter transgene (Figure 2). Furthermore, in DTA⁺ neonates, a significant LysM-Cre–negative alveolar MΦ population was recruited into the pulmonary airspaces. Interestingly, these newly recruited MΦs were not competent to routinely prevent the occurrence of bacterial infections in the emaciated subset of DTA⁺ mice (Figure 4).

The genetic model we have generated is best described as a model of LysM⁺ MΦ depletion coupled to variable recruitment of LysM⁻, functionally defective MΦs or monocytes, rather than a model of complete MΦ depletion. Overall, the patterns observed with this model are consistent with a recent report that identified a large subset of MΦ resistant to LysM-Cre–mediated gene deletion in the peritoneum and liver after inflammatory stimulation (23), and complement other findings showing that mature tissue MΦs and MΦs derived from monocytes are phenotypically distinct (3, 24). Interestingly, in the study of Vannella and colleagues (23), the LysM-Cre–resistant
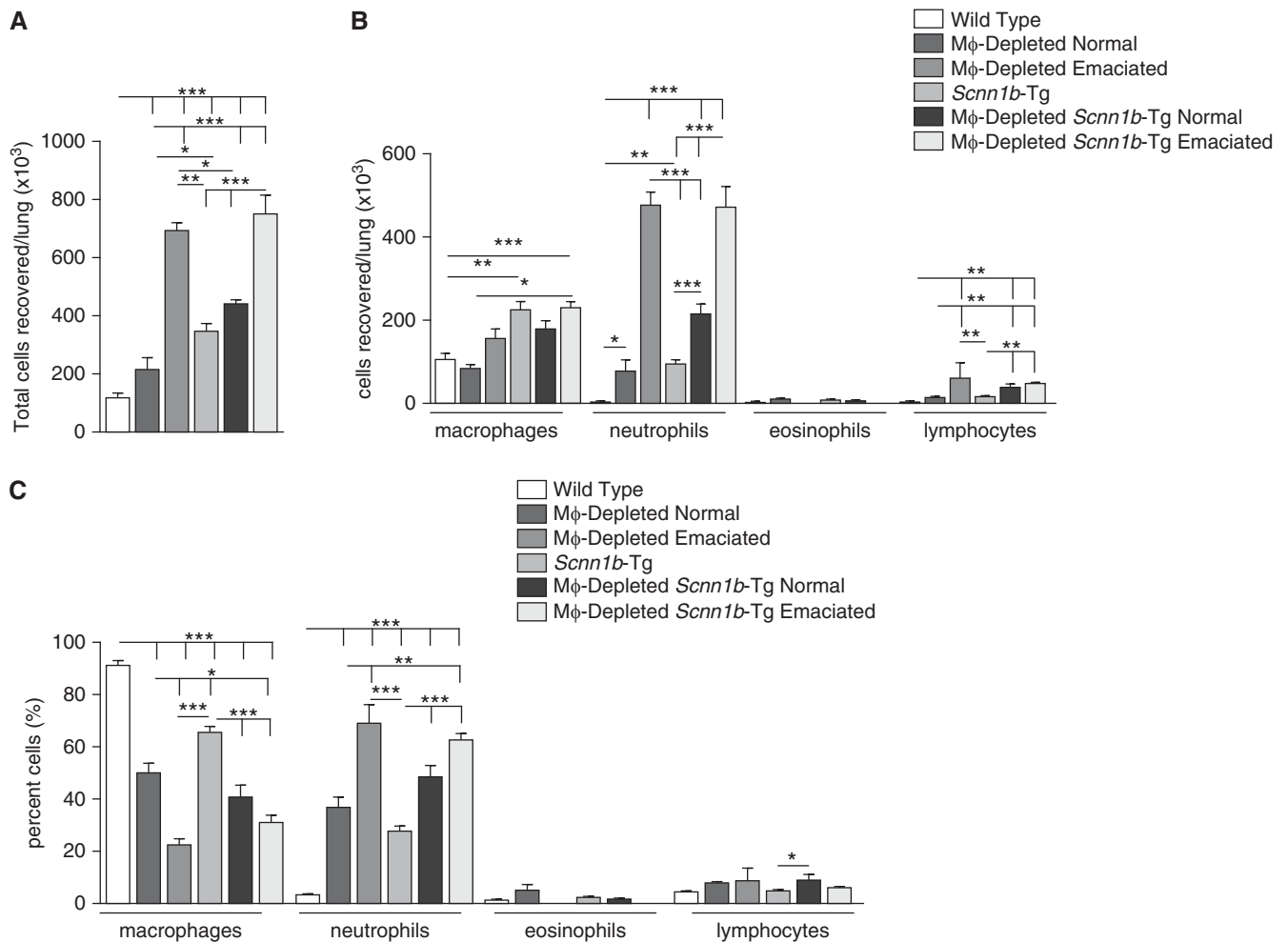
Figure 6. BAL analyses exhibit genotype-specific alteration in total and differential cell counts. (*A*) The BAL cell profile is dependent on MΦ depletion and *Scnn1b*-Tg status. Total (*A*) and differential cell counts (*B*) are shown from BAL cells of neonatal mice for the genotypes, as indicated, and for both emaciated and nonemaciated (normal) neonates. (*C*) Percentage of cell counts are shown from BAL cells of neonatal mice for the genotypes, as indicated, and for both emaciated and nonemaciated (normal) neonates. Data are expressed as means (±SEM). ANOVA: *$P < 0.05$, **$P < 0.01$, ***$P < 0.001$.

MΦs were not characteristic of mature tissue MΦs, and were thought to be more immature with reduced function, consistent with our findings. LysM-Cre–resistant MΦs were also a prominent feature in the pulmonary macrophage population after allergic inflammatory challenge (25). The presence of these Cre-inactive cells is important with respect to the interpretation of results using LysM-Cre technology to delete cells of the myeloid lineage. The breeding strategy applied in our study, using Cre-dependent reporter gene expression coupled to DTA expression (or other lox-flanked alleles), was necessary to interpret the efficiency of LysM Cre–mediated MΦ depletion.

Another feature of our model was the presence of BAL neutrophils associated with

LysM-mediated DTA[+] expression during the neonatal period. This feature is similar to the neutrophilia reported in MAFIA mice, a different model of macrophage depletion (18), and clodronate liposome–induced MΦ depletion (19). Increased neutrophil counts in BAL were also found in a model specifically designed to reduce M2 MΦs using CD206-dependent Cre recombination (26). Kambara and colleagues (26) speculated that the neutrophilia reflected the disruption of the normal antiinflammatory role of M2 macrophage populations. In parallel, proinflammatory mediators derived from DTA[+], apoptotic MΦs also could contribute to this phenomenon (27). MΦs are also critical for clearing apoptotic cells generated during normal lung

development (28), and neutrophil recruitment may be a compensatory mechanism after MΦ depletion in neonatal lungs with LysM-mediated DTA expression. The functional consequences of LysM-mediated DTA expression in the neutrophil populations in our model will require further study.

Spontaneous bacterial infection is one of the consistent features of *Scnn1b*-Tg neonates, with infection due to both gram-positive and gram-negative species (7). These bacteria appear to originate from aspiration from the oral cavity, and are seemingly maintained in the neonatal *Scnn1b*-Tg mice at nonlethal densities due to the poor mucus clearance characteristic of this model. Interestingly, 24% of WT (non–*Scnn1b*-Tg) mice that expressed
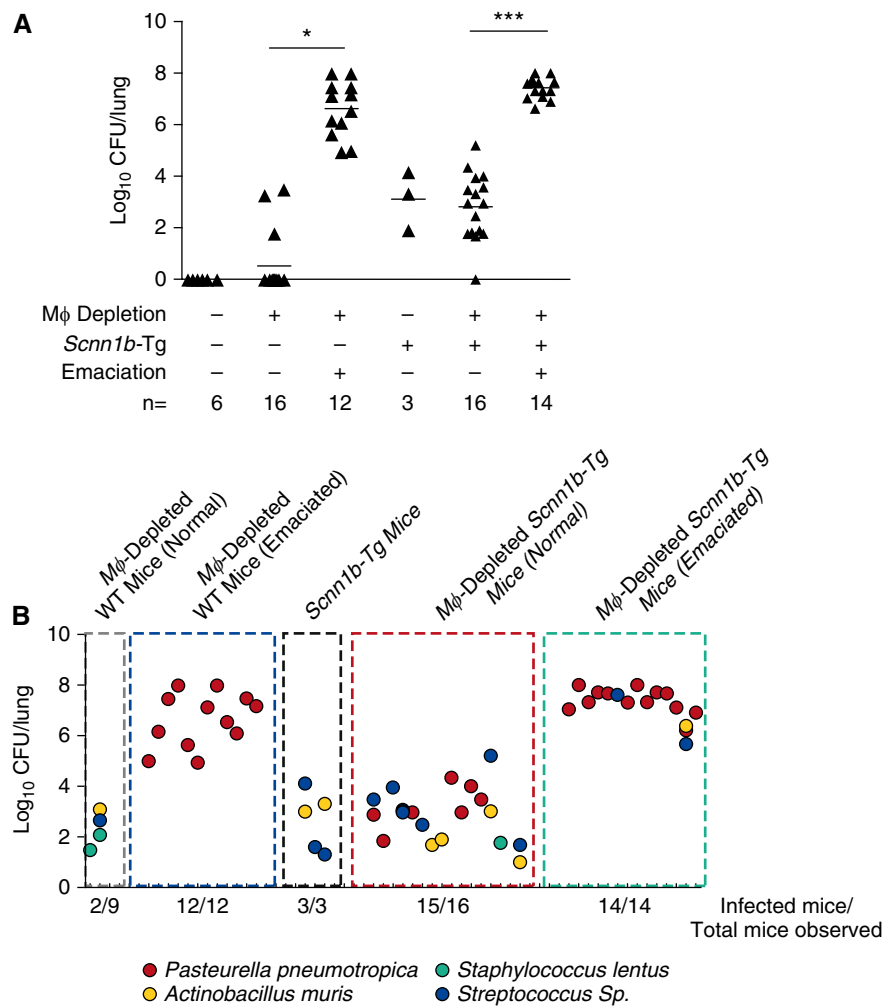
Figure 7. Microbiological analyses of BAL fluid from MΦ-depleted neonates. (A) BAL CFU counts by genotype and emaciation status, as indicated. The CFU values were log10 transformed with an offset of +1 before inferential statistical analyses. This approach enabled the plotting of "zero" CFU values. (B) Bacterial species identification, as determined by 16S ribosomal DNA sequencing of cultured bacteria from BAL. Each *tick* of the *x-axis* represents one mouse within the group. ANOVA: *$P < 0.05$, ***$P < 0.001$.

LysM-mediated DTA expression (i.e., disrupted MΦ function) exhibited lethal emaciation by 2–3 days after birth, associated with alveolar airspace consolidation, neutrophil-dominated inflammation, and a cytokine storm. The frequency of this occurrence increased to 51% in DTA[+]/*Scnn1b*-Tg mice. Strikingly, the only bacterial species identified in the DTA[+]/WT emaciated mice was *Pasteurella pneumotropica*, an opportunistic pathogen of the oropharynx of mice (29), whereas the *Scnn1b*-Tg line exhibited pneumonias with a broader species distribution typical of the species that normally colonize the *Scnn1b*-Tg line. These data support a model whereby mucus clearance (normal in WT mice) is sufficient for clearance of most aspirated bacteria, but that specific bacteria (e.g., *P. pneumotropica*) escape mucus clearance and require a second component of airways defense (i.e., MΦ function) for clearance. Although the mechanism by which *P. pneuomotropica* alone escapes mucus clearance in MΦ-deficient WT mice is not clear, the overall notion of the importance of MΦs in *P. pneuomotropica* clearance is consistent with previous studies reporting that MΦ-specific Toll-like receptor 4 protects against intranasally administered *P. pneumotropica* (30).

Although it is possible that altered neutrophil function due to LysM-Cre–mediated DTA[+] expression in these cells contributed to pneumonia, no evidence of LysM-Cre driven EGFP was observed in BAL neutrophils. Furthermore, in previous studies, near-complete absence of airway neutrophils in *Scnn1b*-Tg neonates, driven by Myd88 deletion, resulted in only approximately 1 log higher bacterial counts and no evidence of emaciation (7), compared with the approximately 5 log increment in bacterial load accompanied by emaciation in this study. Consequently, the bulk of evidence supports a direct effect of MΦ depletion on the prevalence and severity of the bacterial pneumonias in DTA[+]/WT and DTA[+]/*Scnn1b*-Tg mice, consistent with the known role of MΦs during pulmonary bacterial infections (31, 32).

We had predicted that the reduced MΦ function in DTA[+]/*Scnn1b*-Tg mice would reduce the severity of airspace enlargement, given the reported role of MΦ-derived matrix metalloproteinase 12 to the development of this phenotype in the *Scnn1b*-Tg model (33). We speculate that the persistent airspace enlargement may reflect at least two different scenarios. First, raised neutrophil elastase levels mediated by increased neutrophil numbers may have dominated emphysema pathophysiology, producing the observed worsening rather than amelioration of airspace enlargement (34, 35). Second, immature macrophage populations may exhibit protease:antiprotease imbalance with increased protease release (matrix metalloproteinases) or/and decreased antiprotease release (tissue inhibitors of metalloproteinases [TIMPs]) (35, 36).

Mucus plugging typical of WT *Scnn1b*-Tg neonates was almost completely absent in emaciated DTA[+]/*Scnn1b*-Tg mice. Because the mucus plugging in neonatal *Scnn1b*-Tg mice is at least partially related to Th2-type gene responses, the absence of mucus plugging likely reflects the observed shift in cytokine profile due to a high bacterial burden (14). Indeed, both eosinophil numbers and levels of BAL IL-5, a Th2 cytokine known to induce mucus cell metaplasia (37), were significantly reduced in emaciated DTA[+]/*Scnn1b*-Tg mice. The cytokine and cell quantitation data also suggest that emaciated neonates exhibited a neutrophil-dominated Th17 profile, with increased levels of Th17 cytokines (e.g., TNF-α, IL-6, and IL-17). Cross-talk between neutrophils, MΦ apoptosis–induced neutrophilia (27), and Th17 responses (38) enhanced in the presence of bacterial infection likely produced the Th17-dominated inflammation in this scenario.

Our findings that the nonemaciated DTA$^+$/*Scnn1b*-Tg mice exhibit increased inflammation and equivalent mucus plugging as compared with DTA$^-$/*Scnn1b*-Tg mice contrasts with recent findings in models of Th2-type allergic lung inflammation. In the allergic models, MΦ depletion attenuated, rather than enhanced, goblet cell metaplasia and other Th2 inflammatory responses in the absence of bacterial pneumonia (25, 39, 40).

The contrast in results highlights the importance of considering the role of MΦs within the context of the specific disease model being studied. These data also predict that development of therapies directed at MΦ function with indication for multiple pulmonary diseases will not be straightforward.

In conclusion, our genetic approaches to explore the interactions between defects in mucus clearance and macrophage function on pulmonary host defense in mice produced several important observations. First, MΦ depletion led to reduced pulmonary bacterial clearance and alveolar infection in a fraction of WT mice, which became more prevalent in the context of the impaired mucus clearance. Second, the model identified populations of LysM-Cre–inactive alveolar MΦs in multiple contexts, including WT neonatal mice and mucus-obstructed *Scnn1b*-Tg mice, which provides an opportunity to explore the mechanisms leading to monocyte/macrophage recruitment from the blood to the lung across developmental ages and during disease. Third, the failure of macrophage depletion to ameliorate the phenotype in *Scnn1b*-Tg mice demonstrates the complexity of the interplay between defective mucus clearance and macrophage function in muco-obstructive lung diseases. ■

References

1. Cheung DO, Halsey K, Speert DP. Role of pulmonary alveolar macrophages in defense of the lung against *Pseudomonas aeruginosa*. *Infect Immun* 2000;68:4585–4592.
2. Kooguchi K, Hashimoto S, Kobayashi A, Kitamura Y, Kudoh I, Wiener-Kronish J, Sawa T. Role of alveolar macrophages in initiation and regulation of inflammation in *Pseudomonas aeruginosa* pneumonia. *Infect Immun* 1998;66:3164–3169.
3. Hashimoto S, Pittet JF, Hong K, Folkesson H, Bagby G, Kobzik L, Frevert C, Watanabe K, Tsurufuji S, Wiener-Kronish J. Depletion of alveolar macrophages decreases neutrophil chemotaxis to *Pseudomonas* airspace infections. *Am J Physiol* 1996;270: L819–L828.
4. Hackett BP, Gitlin JD. Cell-specific expression of a Clara cell secretory protein–human growth hormone gene in the bronchiolar epithelium of transgenic mice. *Proc Natl Acad Sci USA* 1992;89: 9079–9083.
5. Mall M, Grubb BR, Harkema JR, O'Neal WK, Boucher RC. Increased airway epithelial Na+ absorption produces cystic fibrosis–like lung disease in mice. *Nat Med* 2004;10:487–493.
6. Mall MA, Harkema JR, Trojanek JB, Treis D, Livraghi A, Schubert S, Zhou Z, Kreda SM, Tilley SL, Hudson EJ, *et al*. Development of chronic bronchitis and emphysema in β-epithelial Na+ channel–overexpressing mice. *Am J Respir Crit Care Med* 2008;177:730–742.
7. Livraghi-Butrico A, Kelly EJ, Klem ER, Dang H, Wolfgang MC, Boucher RC, Randell SH, O'Neal WK. Mucus clearance, MyD88-dependent and MyD88-independent immunity modulate lung susceptibility to spontaneous bacterial infection and inflammation. *Mucosal Immunol* 2012;5:397–408.
8. Trojanek JB, Cobos-Correa A, Diemer S, Kormann M, Schubert SC, Zhou-Suckow Z, Agrawal R, Duerr J, Wagner CJ, Schatterny J, *et al*. Airway mucus obstruction triggers macrophage activation and matrix metalloproteinase 12–dependent emphysema. *Am J Respir Cell Mol Biol* 2014;51:709–720.
9. Saini Y, Dang H, Livraghi-Butrico A, Kelly EJ, Jones LC, O'Neal WK, Boucher RC. Gene expression in whole lung and pulmonary macrophages reflects the dynamic pathology associated with airway surface dehydration. *BMC Genomics* 2014;15:726.
10. Kreisel D, Nava RG, Li W, Zinselmeyer BH, Wang B, Lai J, Pless R, Gelman AE, Krupnick AS, Miller MJ. *In vivo* two-photon imaging reveals monocyte-dependent neutrophil extravasation during pulmonary inflammation. *Proc Natl Acad Sci USA* 2010;107: 18073–18078.
11. Clausen BE, Burkhardt C, Reith W, Renkawitz R, Förster I. Conditional gene targeting in macrophages and granulocytes using LysMCre mice. *Transgenic Res* 1999;8:265–277.
12. Muzumdar MD, Tasic B, Miyamichi K, Li L, Luo L. A global double-fluorescent Cre reporter mouse. *Genesis* 2007;45:593–605.
13. Voehringer D, Liang HE, Locksley RM. Voehringer D, Liang HE, Locksley RM. Homeostasis and effector function of lymphopenia-induced "memory-like" T cells in constitutively T cell–depleted mice. *J Immunol* 2008;180:4742–4753.
14. Livraghi A, Grubb BR, Hudson EJ, Wilkinson KJ, Sheehan JK, Mall MA, O'Neal WK, Boucher RC, Randell SH. Airway and lung pathology due to mucosal surface dehydration in beta-epithelial Na$^+$ channel–overexpressing mice: role of TNF-alpha and IL-4Ralpha signaling, influence of neonatal development, and limited efficacy of glucocorticoid treatment. *J Immunol* 2009;182:4357–4367.
15. Livraghi-Butrico A, Grubb BR, Kelly EJ, Wilkinson KJ, Yang H, Geiser M, Randell SH, Boucher RC, O'Neal WK. Genetically determined heterogeneity of lung disease in a mouse model of airway mucus obstruction. *Physiol Genomics* 2012;44:470–484.
16. Byers DE, Holtzman MJ. Alternatively activated macrophages and airway disease. *Chest* 2011;140:768–774.
17. Hussell T, Bell TJ. Alveolar macrophages: plasticity in a tissue-specific context. *Nat Rev Immunol* 2014;14:81–93.
18. Burnett SH, Kershen EJ, Zhang J, Zeng L, Straley SC, Kaplan AM, Cohen DA. Conditional macrophage ablation in transgenic mice expressing a Fas-based suicide gene. *J Leukoc Biol* 2004;75: 612–623.
19. Nakamura T, Abu-Dahab R, Menger MD, Schäfer U, Vollmar B, Wada H, Lehr CM, Schäfers HJ. Depletion of alveolar macrophages by clodronate-liposomes aggravates ischemia–reperfusion injury of the lung. *J Heart Lung Transplant* 2005;24:38–45.
20. Miyake Y, Kaise H, Isono K, Koseki H, Kohno K, Tanaka M. Protective role of macrophages in noninflammatory lung injury caused by selective ablation of alveolar epithelial type II Cells. *J Immunol* 2007; 178:5001–5009.
21. Jakubzick C, Bogunovic M, Bonito AJ, Kuan EL, Merad M, Randolph GJ. Lymph-migrating, tissue-derived dendritic cells are minor constituents within steady-state lymph nodes. *J Exp Med* 2008;205: 2839–2850.
22. Markart P, Faust N, Graf T, Na CL, Weaver TE, Akinbi HT. Comparison of the microbicidal and muramidase activities of mouse lysozyme M and P. *Biochem J* 2004;380:385–392.
23. Vannella KM, Barron L, Borthwick LA, Kindrachuk KN, Narasimhan PB, Hart KM, Thompson RW, White S, Cheever AW, Ramalingam TR, *et al*. Incomplete deletion of IL-4Rα by LysM(Cre) reveals distinct subsets of M2 macrophages controlling inflammation and fibrosis in chronic schistosomiasis. *PLoS Pathog* 2014;10:e1004372.
24. Gundra UM, Girgis NM, Ruckerl D, Jenkins S, Ward LN, Kurtz ZD, Wiens KE, Tang MS, Basu-Roy U, Mansukhani A, *et al*. Alternatively activated macrophages derived from monocytes and tissue

macrophages are phenotypically and functionally distinct. *Blood* 2014;123:e110–e122.

25. Lee YG, Jeong JJ, Nyenhuis S, Berdyshev E, Chung S, Ranjan R, Karpurapu M, Deng J, Qian F, Kelly EA, *et al.* Recruited alveolar macrophages, in response to airway epithelial–derived monocyte chemoattractant protein 1/CCL2, regulate airway inflammation and remodeling in allergic asthma. *Am J Respir Cell Mol Biol* 2014;52:772–784.

26. Kambara K, Ohashi W, Tomita K, Takashina M, Fujisaka S, Hayashi R, Mori H, Tobe K, Hattori Y. *In vivo* depletion of CD206 M2 macrophages exaggerates lung injury in endotoxemic mice. *Am J Pathol* 2015;185: 162–171.

27. Hohlbaum AM, Gregory MS, Ju ST, Marshak-Rothstein A. Fas ligand engagement of resident peritoneal macrophages *in vivo* induces apoptosis and the production of neutrophil chemotactic factors. *J Immunol* 2001;167:6217–6224.

28. Li MO, Sarkisian MR, Mehal WZ, Rakic P, Flavell RA. Phosphatidylserine receptor is required for clearance of apoptotic cells. *Science* 2003;302:1560–1563.

29. Mikazuki K, Hirasawa T, Chiba H, Takahashi K, Sakai Y, Ohhara S, Nenui H. Colonization pattern of *Pasteurella pneumotropica* in mice with latent pasteurellosis. *Jikken Dobutsu* 1994;43:375–379.

30. Hart ML, Mosier DA, Chapes SK. Toll-like receptor 4–positive macrophages protect mice from *Pasteurella pneumotropica*–induced pneumonia. *Infect Immun* 2003;71:663–670.

31. Ghoneim HE, Thomas PG, McCullers JA. Depletion of alveolar macrophages during influenza infection facilitates bacterial superinfections. *J Immunol* 2013;191:1250–1259.

32. Broug-Holub E, Toews GB, van Iwaarden JF, Strieter RM, Kunkel SL, Paine III R, Standiford TJ. Alveolar macrophages are required for protective pulmonary defenses in murine *Klebsiella pneumonia*: elimination of alveolar macrophages increases neutrophil recruitment but decreases bacterial clearance and survival. *Infect Immun* 1997;65:1139–1146.

33. Hautamaki RD, Kobayashi DK, Senior RM, Shapiro SD. Requirement for macrophage elastase for cigarette smoke–induced emphysema in mice. *Science* 1997;277:2002–2004.

34. Gehrig S, Duerr J, Weitnauer M, Wagner CJ, Graeber SY, Schatterny J, Hirtz S, Belaaouaj A, Dalpke AH, Schultz C, *et al.* Lack of neutrophil elastase reduces inflammation, mucus hypersecretion, and emphysema, but not mucus obstruction, in mice with cystic fibrosis–like lung disease. *Am J Respir Crit Care Med* 2014;189: 1082–1092.

35. Stockley RA. Neutrophils and the pathogenesis of COPD. *Chest* 2002; 121(5 suppl)151S–155S.

36. Tetley TD. Macrophages and the pathogenesis of COPD. *Chest* 2002; 121(5 suppl)156S–159S.

37. Lee JJ, McGarry MP, Farmer SC, Denzler KL, Larson KA, Carrigan PE, Brenneise IE, Horton MA, Haczku A, Gelfand EW, *et al.* Interleukin-5 expression in the lung epithelium of transgenic mice leads to pulmonary changes pathognomonic of asthma. *J Exp Med* 1997; 185:2143–2156.

38. Pelletier M, Maggi L, Micheletti A, Lazzeri E, Tamassia N, Costantini C, Cosmi L, Lunardi C, Annunziato F, Romagnani S, *et al.* Evidence for a cross-talk between human neutrophils and Th17 cells. *Blood* 2010;115:335–343.

39. Mathie SA, Dixon KL, Walker SA, Tyrrell V, Mondhe M, O'Donnell VB, Gregory LG, Lloyd CM. Alveolar macrophages are sentinels of murine pulmonary homeostasis following inhaled antigen challenge. *Allergy* 2015;70:80–89.

40. Zasłona Z, Przybranowski S, Wilke C, van Rooijen N, Teitz-Tennenbaum S, Osterholzer JJ, Wilkinson JE, Moore BB, Peters-Golden M. Resident alveolar macrophages suppress, whereas recruited monocytes promote, allergic lung inflammation in murine models of asthma. *J Immunol* 2014;193: 4245–4253.